

Electrochemical Behavior and Corrosion Products of Casing Steel under CO₂ Condition

Longting Wang^{1,2,*}, Liping Sun², Jichuan Kang^{2,3}, Baoping Cai¹, Yanfu Wang¹ and Yaonan Wu¹

¹ College of Mechanical and Electronic Engineering, China University of Petroleum (East China), Qingdao 266000, China

² College of Shipbuilding Engineering, Harbin Engineering University, Harbin 150000, China

³ Center for Marine Technology and Engineering, University of Lisbon, Portugal

*E-mail: wanglt@upc.edu.cn

Received: 7 July 2019 / Accepted: 8 September 2019 / Published: 29 October 2019

The anodic reaction of CO₂ corrosion of steel is closely related to the formation and characteristics of the corrosion product film. However, the relationship between the anodic reaction and the corrosion product film has not been studied. As a useful tool to study the dynamic process of the electrode and the electrode surface state, the measurement technique of AC impedance has been gradually used to study the characteristics of the CO₂ corrosion product film along with evaluating corrosion inhibitors and ion adsorption on the electrode surface of casing steel. In this work, the AC impedance characteristics of N80 steel in different media environments were studied using. The influence of the electrode reaction and corrosion product film on the AC impedance spectrum is analyzed, and a theoretical model of CO₂ corrosion is proposed. This model is used to study the influence of temperature and Cl⁻ concentration on the impedance spectrum of the cathode and anode of N80 casing steel, to explore the film formation on the surface of the sample and the electrode reaction process and to understand the impact of environmental factors on CO₂ corrosion.

Keywords: Corrosion; Corrosion products; Carbon dioxide; Casing steel; Electrochemical polarization

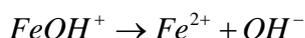
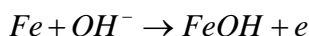
1. INTRODUCTION

The service behavior of oil pipelines includes mechanical behavior, environmental behavior and composite behavior. Failure occurs when components lose their original functions due to deformation, fracture and surface damage under specific service conditions [1–8]. Corrosion plays an important role in petroleum pipeline engineering. The statistical analysis shows that 70% of failure is related to corrosion. Corrosion accidents in oil and gas fields often cause great economic losses, including catastrophic accidents and environmental pollution [9–19]. For example, in 1988, the UK Alpha offshore platform exploded due to corrosion damage, killing 166 people and reducing the annual output of north

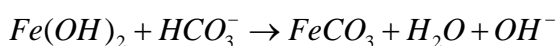
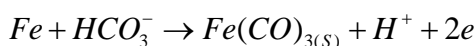
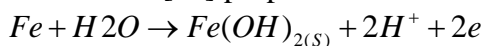
sea oil fields by 12%. On October 26, 1984, the underground pipeline of Uissnk in northern Russia was corroded and broken, causing a large amount of oil leakage and serious environmental pollution. If the anti-corrosion technology is used properly 30~40% of the corrosion loss can be recovered. It can be seen that strengthening corrosion and protection research can bring great economic benefits to the petroleum industry [20–25].

Most petroleum pipes work in a CO₂ environment [26–36]. CO₂ has two main sources. The first one is in nature with the abundant natural CO₂ gas deposits in geological structures. When oil and gas are mined, CO₂ is used as the associated gas output. Second, using multistage miscible CO₂ flooding technology, CO₂ and miscibility of crude oil can cause oil swelling, significantly reducing the viscosity of crude oil and enhancing the oil liquid. The ultimate recovery of a reservoir injected with CO₂ is 15 ~ 20% higher than that of a reservoir injected with fresh water.

Thus far, there is no unified understanding of anodic reactions in CO₂ processes. Waard et al [37] believed that in CO₂ solution, the anodic reactions were:

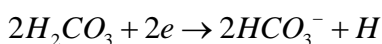


Davies et al [38] proposed different anodic reactions:

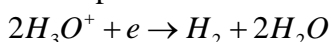


The reasons for the above differences are mainly due to the small understanding of CO₂ corrosion intermediates and the lack of experimental proof.

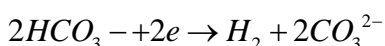
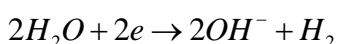
In the process of CO₂ corrosion, the cathodic reaction process controls the corrosion rate of steel. The cathodic reaction process mainly involves the reduction of H⁺, H₂O, H₂CO₃ and HCO₃⁻. Initially, Waard et al [37] believed that only H₂CO₃ was reduced to generate H₂ and HCO₃⁻ in the CO₂ corrosion cathode reaction:



Schmitt [39] suggested that both H⁺ and H₂CO₃ could be reduced at the electrode and the H⁺ reduction is expressed as:



Ogundele [40] proposed that the cathodic process included the reduction of H₂O and HCO₃⁻:



The cathodic reduction is controlled by the diffusion of HCO₃⁻. Nestic et al [41] further believed that when the solution pH < 4, H⁺ reduction dominated the cathodic process and the reaction rate was controlled by diffusion; when the solution had a pH between 4-6, H₂CO₃ and HCO₃⁻ were mainly reduced and the reaction rate was controlled by activation. The H₂O reduction became the main part of the cathodic reaction only when the cathode overpotential was high. It can be seen from the above data

reports that the reduction of H_2CO_3 or HCO_3^- serves as an additional cathodic reaction, and there is still some debate on whether it will play a dominant role in the cathodic process.

At present, the important role of the CO_2 corrosion products film has been widely accepted. The corrosion product film is dense, stable and has a good adhesion force that provides an effective protection effect on the base metal and determines the corrosion rate. At low temperature, the corrosion product film does not easily form on the metal surface, so the corrosion type is uniform corrosion. In the middle temperature region, a porous and loose corrosion product film is formed on the metal surface. On the one hand, the corrosion rate is high; on the other hand, a serious pitting phenomenon will occur. In the high-temperature region, a dense corrosion product film with a strong adhesion force will be formed, and the corrosion rate will be greatly reduced. The corrosion type is uniform corrosion. When the corrosion product film is formed on the material surface, the corrosion rate of CO_2 is determined by the properties of the corrosion product film. Therefore, studying the formation conditions, structural characteristics, mechanical properties, chemical stability and other aspects of corrosion product films will be helpful for understanding the diversity and complexity of the CO_2 corrosion rate and corrosion morphology.

To further understand the influence of the corrosion product film on the corrosion rate and corrosion morphology, there are still many problems that need to be studied deeply. In this paper, we studied the film structure and microstructure evolution of corrosion products for ordinary casing steel. The relationship between the characteristics of the corrosion product film and the electrode reaction, especially the anodic dissolution reaction, was further discussed. This will help to understand the mechanism of film formation of corrosion products. The electrochemical characteristics of CO_2 corrosion were studied to reveal the relationship between the corrosion mechanism and film formation of corrosion products. The mechanism of CO_2 corrosion under the conditions of activation and a corrosion product film covering is mainly studied using ac impedance technology to understand the relationship between the electrode surface state and electrode reaction process.

2. EXPERIMENTAL

N80 tubing steel was used for the study, and its chemical composition is shown in Table 1. The electrochemical samples used were round pieces with a thickness of 4 mm and a diameter of 15 mm. The samples were embedded in the wood powder and connected to the outside world by wires.

A dynamic autoclave was used to simulate the conditions. A saturated calomel electrode (SCE) was used as the reference electrode. Graphite electrodes were used as auxiliary electrodes. All electrochemical tests were completed by an EG-G M237A potentiostat with a M5210 phase-locked amplifier.

The tubing samples were first polished step by step with 220#, 400#, 600#, and 1000# water sandpaper and then washed with distilled water and acetone. NaCl solution was prepared with a pure analytical chemical reagent and distilled water. The concentration of the experimental medium for the anodic and cathodic reactions was 0.5 M NaCl, 0.5 M NaCl+0.001 M HCl, and 0.5 M NaCl+0.1 M Na_2CO_3 . Before the experiment, high-pure N_2 (2 h) was used to deoxygenate, and then high-pure CO_2

was used to saturate the medium. Electrochemical measurements were performed after the electrode was stabilized. The electrochemical impedance test was completed using M398 software. The test frequency range was 5 mHz-100 kHz. The polarization curve test of dynamic potential scanning was 0.1 mV/s.

Table 1. Chemical composition of N80 steel (wt%).

C	Si	Mn	P	S	Cr	Mo	Ni	Nb	V	Ti	Cu
0.242	0.221	1.196	0.012	0.004	0.036	0.022	0.020	0.028	0.016	0.010	0.017

3. RESULTS AND DISCUSSION

Figure 1A shows the polarization curves of N80 steel measured under different media conditions. It can be seen from the figure that N80 steel has the highest anodic dissolution rate in 0.5 M NaCl+0.001M HCl medium. It can be seen that the N80 steel in 0.5 M NaCl (-720 mV) and 0.5 M NaCl+0.1 M Na₂CO₃ (-750 mV) showed similar corrosion potential, while the N80 steel in 0.5 M NaCl+0.001 M HCl had a lower corrosion potential (-612 mV). In general, the passive current density (I_{pass}) and pitting potential are usually employed to evaluate the corrosion resistance quantitatively for a spontaneous passive system. In this work, no pitting corrosion is detected for all conditions. Therefore, only the I_{pass} is used, which was obtained at 0.5 V. For an active system, I_{corr} is usually used to assess the corrosion resistance, which can be obtained directly by extrapolating the anodic and cathodic Tafel lines to the open-circuit corrosion potential (E_{corr}) [42]. It can be seen that cathodic Tafel slope values of the N80 steel in 0.5 M NaCl, 0.5 M NaCl+0.1 M Na₂CO₃ and 0.5 M NaCl+0.001 M HCl are close to -112 mV/decade, -114 mV/decade and -133 mV/decade, respectively.

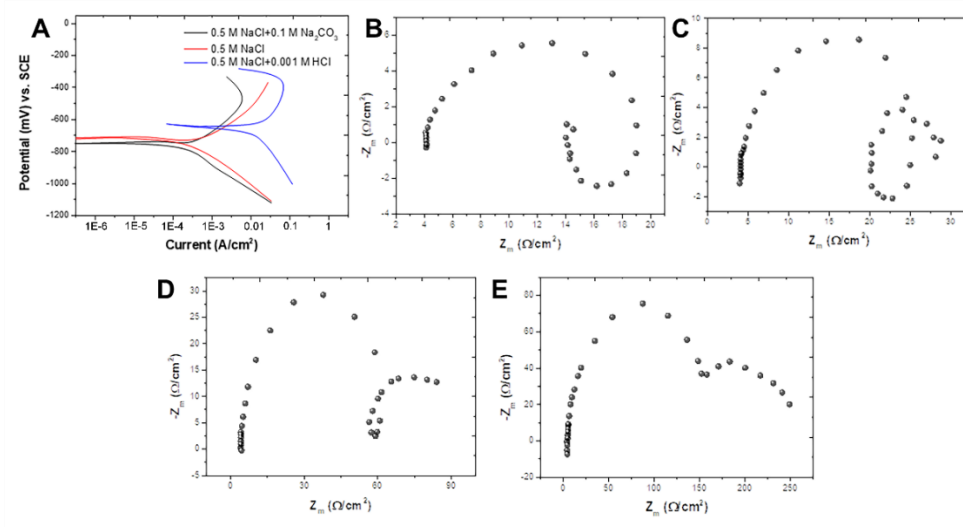


Figure 1. (A) Polarization curves of N80 steel in various electrolytes at 60 °C. The Nyquist plots for the corrosion of N80 steel in CO₂ saturated solution at 60 °C. (B) 0.5 M NaCl+0.001 M HCl, (C) 0.5 M NaCl, (D) 0.5 M NaCl+0.1 M HCl and (E) pre-polarized in 0.5 M NaCl+0.1 M Na₂CO₃ at 60 °C.

At the end of the experiment, no corrosion products are attached to the sample. A layer of loose black corrosion products is formed on the surface of the sample, in which some bright active points are distributed. In the 0.1 M NaCl+0.1 M Na₂CO₃ solution, the corrosion rate was the lowest, and the coverage of corrosion products was relatively dense and thick, leading to passivation in the polarization curve. As the previous study reported that as for corrosion resistance steel or alloys, the radius of the semi-circular arc is related to the polarization resistance of the passive film [43–45].

So far, many equivalent circuit models have been chosen to explain the impedance data on passive film in the solution [46,47]. Figure 1B shows the Nyquist curve measured under the anode overpotential of 50 mV with different media conditions. At this time, the main reaction of the ac impedance map is the Faraday impedance of the anode.

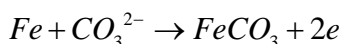
Figure 1C shows the Nyquist plots measured in 0.5 M NaCl + 0.001 M HCl solution with saturated CO₂. It can be seen from the figure that the EIS curve has two regions, namely, the capacitive reactance arc in the high-frequency region and the inductive reactance arc in the low-frequency region. Under this medium condition, the surface of the sample is not easy to obtain from the film. After the end of the experiment, the surface of the sample was observed, and it could be seen that most areas of the sample surface were not covered by the corrosion product film and were in the activated state. It is believed that the passive film has a capacitive character or the structure of the passive film has both compact outer layer and inner layer [48].

Figure 1D shows the Nyquist plots measured in 0.5 M NaCl solution saturated with CO₂. The EIS curve has three time regions, including the capacitive and reactance arc in the high-frequency region, the reactance arc in the low-frequency region and the reactance arc. At the end of the experiment, most areas of the surface of the sample were covered by black corrosion products, and the active areas existed as dots.

Figure 1D shows the Nyquist curve measured in a CO₂ saturated solution of 0.5 M NaCl + 0.1 M Na₂CO₃. The EIS curve still has three regions, but the inductive arc shrinks and the capacitive arc expands in the low-frequency region. Anodic dissolution might leave behind clusters of atomic vacancies that diffuse into the steel, and have been considered as a driver for softening behavior [49]. At the end of the experiment, the surface of the sample was covered by black corrosion products, and the active point was difficult to observe.

In Figure 1E, the Nyquist plots were measured in 0.5 M NaCl+ 0.1 M Na₂CO₃ solution with CO₂ saturation, and the polarization potential was 100 mV (relative to the self-corrosion potential). There are only two regions in the EIS curve, where the inductive arc disappears in the low-frequency region and the capacitive arc expands further. At the end of the experiment, the surface of the sample was completely covered by black corrosion products.

The anodic reactions of the casing steel CO₂ corrosion process are as follows:



The three reactions can be carried out from the thermodynamic point of view, and the first and second reactions easily lead to the formation of corrosion product films on the surface of the sample. At

the same time, the Fe^{2+} from the third reaction diffuses into the solution. It can be seen from the polarization curve in Figure 1A that when the concentration of CO_3^{2-} in the solution increases, the speed of the first reaction accelerates, making the surface of the sample easy to form a film, leading to passivation. When the concentration of H^+ in the solution increases, on the one hand, the surface of the sample is not easy to form a film; on the other hand, the concentration of CO_3^{2-} and HCO_3^- in the solution is greatly reduced. The mechanistic investigations on this subject have been generally focused on the cathodic reactions of this system, whereas the effect of CO_2 on the anodic iron dissolution reaction in acidic solutions was not investigated in much depth [50]. According to the Nernst formula, this will increase the equilibrium potential of the first and second reactions and decrease the reaction driving force. In this case, the anodic dissolution is dominated by the third reaction.

The occurrence of the inductive and capacitive arcs of the EIS curve in the low-frequency region of the anode area is closely related to the surface state of the sample, so it can be considered that the occurrence of the inductive arc in the low-frequency region is related to the activation and dissolution of the noncorrosive product film that covers an area of the sample surface. The reactance arc is dissolved in the film covering the area of corrosion products on the surface of the sample. The significant increase of the anodic reaction rate in the transition and pre-passivation ranges are found to be in agreement with the results reported previously by Linter and Burstein [51]. At the same time, the film coverage of the corrosion products on the surface of the sample is related to the reaction rates of the first and second anodes. When the reaction rate of the first and second anodes is high, the corrosion product film easily forms on the surface of the sample. Meanwhile, the inductive arc of the low-frequency region of the EIS curve will shrink, and the capacitive arc will expand. When the reaction rate of the third anode is higher, the film coverage of corrosion products on the surface of the sample will be smaller. Meanwhile, the inductive arc of the EIS curve in the low frequency region is obvious, while the capacitive arc is small.

Figure 2A shows the cathode polarization curve of N80 steel under different medium conditions. As seen from the figure, adding HCl and NaHCO_3 to a NaCl solution saturated with CO_2 significantly increases the cathodic reduction current density, which reflects that both H^+ and HCO_3^- are involved in the cathodic reduction process, so increasing the concentration of H^+ or HCO_3^- will increase the cathodic current density. Keddam et al. suggest that the increased current after the first maximum is a result of a parallel reaction pathway involving Fe(II) intermediate species [52,53]. The second current maximum at more positive potentials leading to the surface passivation (not observed in the polarization curves presented above), was associated with a chemical transformation of Fe(II) intermediates to insoluble passivating species. In the aqueous solution of $\text{NaCl} + \text{HCl} + \text{CO}_2$, H^+ reduction is given priority, and the cathodic polarization curve appeared to be the limiting current density caused by the H^+ diffusion control. In the aqueous solution of $\text{NaCl} + \text{NaHCO}_3 + \text{CO}_3$, HCO_3^- reduction is the main cathodic reaction. The reaction is controlled by activation. In a saturated CO_2 NaCl solution, the cathodic polarization curve of the Tafel slope is 0.394 V/dec, showing that under the condition of the cathode reaction not only the reduction of HCO_3^- and H^+ occurs but also other cathode reactions also participated.

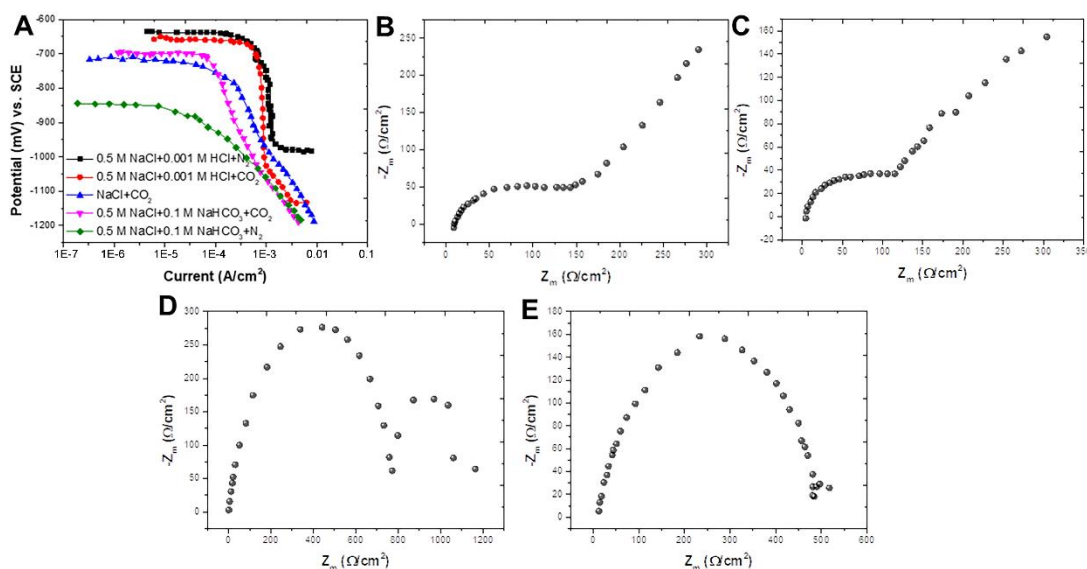


Figure 2. (A) Cathodic polarization curves of N80 steel in various electrolytes at 30 °C. The Nyquist plots of N80 steel in CO₂ saturated solution at 30 °C. (B) 0.5 M NaCl+0.001 M HCl, (C) 0.5 M NaCl+0.001M HCl+CO₂, (D) 0.5 M NaCl+CO₂ and (E) 0.5 M NaCl+0.1 M NaHCO₃+CO₂.

Under the condition shown in Figure 2A, due to only H⁺ reduction in solution, the reaction is controlled by diffusion, and typical impedance characteristics of Warburg appear in the ac impedance spectrum.

Under the condition shown in Figure 2B, the impedance spectrum in the low-frequency region is superposed by Warburg impedance and capacitive reactance, indicating that the cathodic reduction process has diffusion control and activation control characteristics at the same time. The reduction of H⁺ is controlled by diffusion, while the reduction of H₂CO₃ and HCO₃⁻ is characterized by activation control. When there are two reduction reactions for activation control in the cathodic process, Faraday impedance shows the characteristics of capacitive reactance, indicating that the reduction of H₂CO₃ and HCO₃⁻ is an additional cathodic reduction reaction, which makes the low-frequency region of the impedance spectrum have the characteristics of capacitive reactance. Therefore, under the condition shown in Figure 2C, the cathodic reduction reaction is dominated by H⁺, while the reduction of H₂CO₃ and HCO₃⁻ is relatively secondary.

Under the condition shown in Figure 2D, the ac impedance has the characteristics of double capacitive reactance. This indicated that the reduction of H₂CO₃ and HCO₃⁻ was mainly controlled by activation. From the perspective of the ac impedance spectrum, Warburg impedance characteristics no longer exist in the low frequency region. Therefore, H⁺ reduction is no longer a major part of the cathodic reaction.

Under the condition shown in Figure 2E, the concentration of HCO₃⁻ in the solution increases greatly, and the reduction speed of HCO₃⁻ also increases, so that only a single capacitive arc reactance characteristic appears in the ac impedance range.

Figure 3 shows the anode impedance spectra of N80 steel measured in 0.5 M CO₂ saturated NaCl solution at 30 °C, 60 °C and 90 °C. The curve fitting results are shown in Table 2. Because the cathodic

reaction is the control step of the speed in the CO₂ corrosion process, the anodic reaction speed is much higher than the cathodic reaction speed. In this way, even when measured at the self-corrosion potential, the results still reflect the characteristics of the anodic reaction.

As shown in the figure, the inductive arc in the ac impedance spectrum shrinks gradually with increasing temperature. The shrinkage of the inductive arc is related to the surface state of the sample; that is, when the anodic reaction speed of $Fe+CO_3^{2-}=FeCO_3+2e$ is large, the surface of the sample easily forms the corrosion product film. The inductive arc of the low-frequency region of the EIS curve will shrink, and the capacitive arc will expand. When the anodic reaction rate of $Fe=Fe^{2+}+2e$ is high, the film coverage of corrosion products on the sample surface will be small.

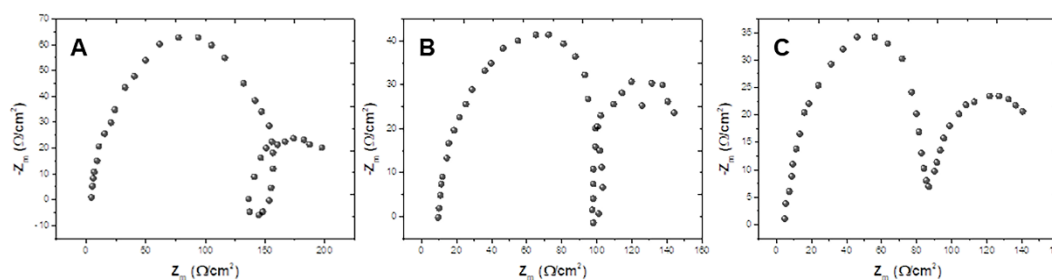


Figure 3. The Nyquist plots of N80 steel in 0.5 M NaCl solution saturated with CO₂ at (A) 30 °C (B) 60 °C and (C) 90 °C.

Table 2. Fitting results of the anodic impedance spectra of N80 steel at different temperatures in 0.5 M NaCl solution saturated with CO₂.

T	Rs (Ω/cm ²)	C _{dl} (F/cm ²)	R _t (Ω/cm ²)	R _L (Ω/cm ²)	C (F/cm ²)	R _c (Ω/cm ²)
30 °C	3.47	7.21 x 10 ⁻⁴	160.43	670.32	0.22	77.68
60 °C	9.87	5.88 x 10 ⁻⁴	116.24	586.32	0.71	63.79
90 °C	5.20	1.08 x 10 ⁻³	100.56	435.62	0.31	64.51

Figure 4 shows the anodic impedance spectra of N80 steel measured at 90 °C in NaCl solution with different concentrations of saturated CO₂. At 90 °C, due to the easy film formation on the surface of the sample, the corrosion product film has large surface coverage, so the capacitive and reactance arc in the low-frequency region is obvious, while the inductive reactance arc related to activation and dissolution basically disappears.

In a 0.1 M NaCl solution, the fitting results show that the anodic impedance spectrum is composed of two capacitive reactance arcs, and no inductive reactance property is superimposed in the impedance spectrum. This indicates that the corrosion product film is completely covered on the surface of the sample. In 0.5 M and 2.5 M NaCl solution, the fitting results show that the anodic impedance spectrum already exists in the inductance nature as an impedance spectrum superposition with the increase in the concentration of NaCl. The inductive reactance property in the impedance spectrum is gradually obvious, indicating that the surface active area of the samples increases gradually with

increasing Cl^- concentration. The presence of Cl^- will destroy the coating of corrosion product film on the sample surface. Moreover, in the area where the corrosion product film is not covered, the Cl^- catalytic mechanism enables the anode to be activated and dissolved.

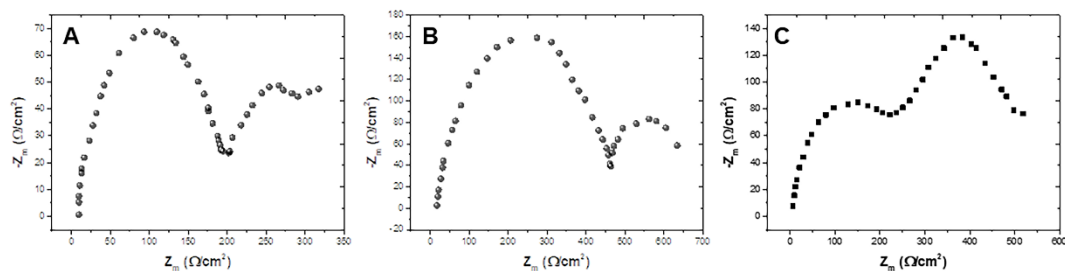


Figure 4. The Nyquist plots of N80 steel in (A) 0.1 M, (B) 0.5 M and (C) 2.5 M NaCl solution saturated with CO_2 .

Figure 5 shows the N80 steel cathodic impedance spectroscopy measurements under different temperature conditions in 0.5 M NaCl solution with saturated CO_2 . As shown in the figure, under the condition of different temperatures, the cathodic impedance spectrum is composed of two capacitive reactance arcs, suggesting that the H_2CO_3 and HCO_3^- reduction reaction is the main characteristic of the cathodic electrode reaction. The temperature will not affect the cathodic reaction type and only affects the cathodic reaction speed.

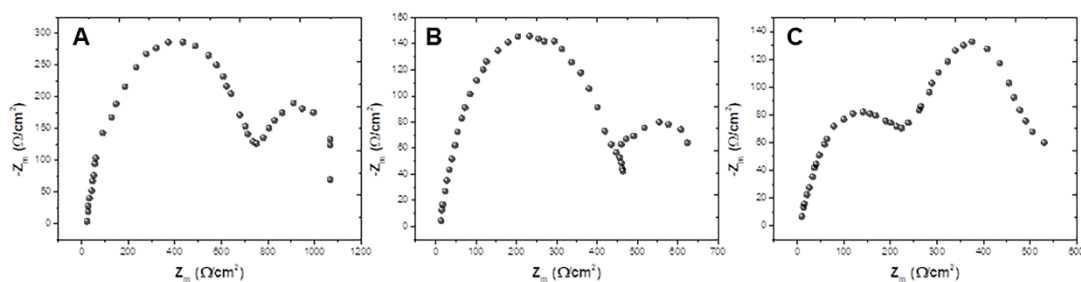


Figure 5. The Nyquist plots of N80 steel at -50 mV in 0.5 M NaCl solution saturated with CO_2 at (A) 30 °C (B) 60 °C and (C) 90 °C.

Figure 6 shows the cathodic impedance spectra of N80 steel measured at 30 °C in different concentrations of NaCl solution with saturated CO_2 . With the increase of Cl^- concentration, the cathodic impedance spectrum is always composed of double capacitive arc reactance, indicating that the cathodic reduction mechanism has not changed. Therefore, the reduction reaction of H_2CO_3 and HCO_3^- is the main cathodic electrode reaction. The transfer resistance R_t and polarization resistance R_p increase gradually, which proves that the reaction rate of cathodic reduction decreases. This may be because after the concentration increases, Cl^- gradually occupies the active position of the cathode, reducing the opportunities for H_2CO_3 and HCO_3^- to participate in the reduction, making the cathodic reduction rate slower.

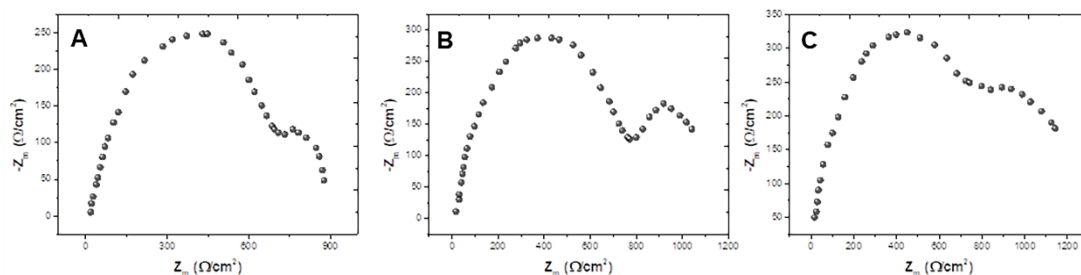


Figure 6. The Nyquist plots of N80 steel at -50 mV in (A) 0.1 M, (B) 0.5 M and (C) 2.5 M NaCl solution saturated with CO₂.

4. CONCLUSION

In conclusion, the EIS spectra of N80 casing steel with CO₂ corrosion have three regions in which a low-frequency inductive arc is related to the activation and dissolution of the sample surface, and a low-frequency capacitive arc is related to the formation of corrosion product film on the sample surface. As the film coverage of corrosion products on the sample surface increases, the inductive arc of the low-frequency region of the EIS curve gradually shrinks. At the same time, the capacitive arc of the reactance gradually expands until only the capacitive arc remains in the low frequency region. At this point, the surface of the sample will be completely covered by a dense corrosion product film. The film formation of corrosion products on the surface of the sample is related to the reaction process of the electrode. The changes in arc resistance and capacitive arc resistance can be inferred from the reaction process of the electrode and film formation of the sample surface. The temperature will significantly increase the reaction rate of CO₂ corrosion of the cathode and anode electrodes, but at the same time, it is easy to form corrosion product films on the surface of the sample to protect the base metal. With increasing Cl⁻ concentration, the dissolution rate of the anode first increases and then decreases. The cathodic reduction rate decreases slowly. The Cl⁻ can destroy the coating of corrosion product film on the surface of the sample and accelerate the dissolution of metal in the active zone.

ACKNOWLEDGMENTS

The authors wish to acknowledge the financial support of National Natural Science Foundation of China (No. 51779267), the Fundamental Research Funds for the Central Universities (No. 17CX02062 and No. 19CX02025A).

References

1. D. Liu, J. Chen, L. Shuai and C. Wei, *Autom. Constr.*, 89 (2018) 24.
2. A.G. Urbina and A. Aoyama, *J. Loss Prev. Process Ind.*, 45 (2017) 116.

3. S. Shin, Lee G, Ahmed U, Lee Y, Na J and Han C, *J. Hazard. Mater.*, 342 (2017) 279.
4. Z. Qu, Y. Wang, H. Yue, A. Yang, L. Wu, W. Zhou, H. Wang, Z. Su, L. Jian and Z. Yu, *J. Loss Prev. Process Ind.*, 47 (2017) 1.
5. Y. Zhou, J. Gong and P. Wang, *Asia-Pac. J. Chem. Eng.*, 11 (2016) 108.
6. L. Yun, S. Han and J. Zhang, *Fuel Process. Technol.*, 146 (2016) 20.
7. Y. Bao, J. Zhang, X. Wang and W. Liu, *Rsc Adv.*, 6 (2016) 80529.
8. L. Fu, A. Wang, G. Lai, C.-T. Lin, J. Yu, A. Yu, Z. Liu, K. Xie, W. Su, *Microchim. Acta*, 185 (2018) 87.
9. L. Fang, Y. Bo, J. Li, Z. Yu, G. Yu and W. Zhao, *Heat Transf. Eng.* (2017) 1.
10. N. Choquettelevy, M. Zhong, H.L. Maclean and J.A. Bergerson, *Environ. Sci. Technol.*, 52 (2017) 337.
11. R. Xiao, G. Xiao, B. Huang, J. Feng and Q. Wang, *Eng. Fail. Anal.*, 68 (2016) 113.
12. R. Mendes, G. Vinay and P. Coussot, *Energy Fuels*, 31 (2016) 395.
13. Y. Liu, Z. Bo, Y. Zhang, L. Ma and Y. Ping, *Eng. Fail. Anal.*, 60 (2016) 307.
14. L. Fu, K. Xie, A. Wang, F. Lyu, J. Ge, L. Zhang, H. Zhang, W. Su, Y.-L. Hou, C. Zhou, C. Wang, S. Ruan, *Anal. Chim. Acta*, 1081 (2019) 51.
15. F. Borfecchia, G.D. Canio, L.D. Cecco, A. Giocoli, S. Grauso, L.L. Porta, S. Martini, M. Pollino, I. Roselli and A. Zini, *Nat. Hazards*, 81 (2016) 759.
16. L. Fu, Z. Liu, J. Ge, M. Guo, H. Zhang, F. Chen, W. Su, A. Yu, *J. Electroanal. Chem.*, 841 (2019) 142.
17. D. Han, Y. Bo, W. Yi, Z. Yu and G. Yu, *Appl. Therm. Eng.*, 88 (2015) 217.
18. A.L. Balogun, A.N. Matori and A.I. Hamid-Mosaku, *Environ. Earth Sci.*, 74 (2015) 1.
19. L. Fu, A. Wang, F. Lyu, G. Lai, J. Yu, C.-T. Lin, Z. Liu, A. Yu, W. Su, *Sens. Actuators B Chem.*, 262 (2018) 326.
20. L. Fu, A. Wang, W. Su, Y. Zheng, Z. Liu, *Ionics*, 24 (2018) 2821.
21. I.P. Shabalov, V.G. Filippov, O.N. Chevskaya and L.A. Baeva, *Metallurgist*, 61 (2017) 463.
22. Q.L. Cheng, Y.F. Gan, S.U. Wen-Kun, S.S. Wang, W. Sun and Y. Liu, *J. Eng. Thermophys.*, 38 (2017) 475.
23. H. Pouraria, J.K. Seo and J.K. Paik, *Ocean Eng.*, 122 (2016) 105.
24. S. Peerapornlerd, S. Edvik, A.P. Leandro, R. Hinckley, M.D. Deo, R. Venkatesan and J.J. Magda, *Ind. Eng. Chem. Res.*, 54 (2015) 15.
25. T. Kumar, A.K. Gautam, B.K. Kanaujia and K. Rambabu, *Electron. Lett.*, 51 (2015) 1626.
26. X. Shi, Y. Wei, D. Xu, M. Yan, C. Yang, Y. Shan and Y. Ke, *J. Mater. Sci. Technol.*, 34 (2018) 258.
27. H.M. Nykyforchyn and A.R. Lysyk, *Mater. Sci.*, 53 (2017) 1.
28. H.M.A. El-Lateef, A.M. Abu-Dief and M.A.A. Mohamed, *J. Mol. Struct.*, 1130 (2017) 522.
29. O. Shabarchin and S. Tesfamariam, *J. Loss Prev. Process Ind.*, 40 (2016) 479.
30. L. Fu, A. Wang, F. Lyv, G. Lai, H. Zhang, J. Yu, C.-T. Lin, A. Yu, W. Su, *Bioelectrochemistry*, 121 (2018) 7.
31. H. Pouraria, J.K. Seo and J.K. Paik, *Ocean Eng.*, 122 (2016) 105.
32. C.I. Ossai, B. Boswell and I. Davies, *Eng. Fail. Anal.*, 60 (2016) 209.
33. H. Hu and Y.F. Cheng, *J. Pet. Sci. Eng.*, 146 (2016) 134.
34. L. Fu, Y. Xu, J. Du, D. Cao, Q. Liu, *Int. J. Electrochem. Sci.*, 14 (2019) 4383.
35. Y. Chen, Z. Hong, J. Zhang, X. Liu, L. Xin and Z. Jing, *Eng. Fail. Anal.*, 47 (2015) 67.
36. Y. Chen, Z. Hong, J. Zhang, L. Xin and Z. Jing, *Mater. Des.*, 67 (2015) 552.
37. C. De Waard and D. Milliams, *Corrosion*, 31 (1975) 177.
38. D. Davies and G. Burstein, *Corrosion*, 36 (1980) 416.
39. G. Schmitt and M. Horstemeier, *NACE International*, 11 (2006) 76.
40. L. Fu, Y. Zheng, P. Zhang, H. Zhang, M. Wu, H. Zhang, A. Wang, W. Su, F. Chen, J. Yu, W. Cai, C.-T. Lin, *Bioelectrochemistry*, 129 (2019) 199.

41. L. Fu, A. Wang, G. Lai, W. Su, F. Malherbe, J. Yu, C.-T. Lin, A. Yu, *Talanta*, 180 (2018) 248.
42. Z.B. Wang, H.X. Hu, Y.G. Zheng, W. Ke and Y.X. Qiao, *Corros. Sci.*, 103 (2016) 50.
43. H. Luo, H. Su, C. Dong and X. Li, *Appl. Surf. Sci.*, 400 (2017) 38.
44. H. Luo, S. Gao, C. Dong and X. Li, *Electrochimica Acta*, 135 (2014) 412.
45. C. Liu, Q. Bi, A. Leyland and A. Matthews, *Corros. Sci.*, 45 (2003) 1257.
46. J. Lv and H. Luo, *J. Nucl. Mater.*, 452 (2014) 469.
47. C. Boissy, C. Alemany-Dumont and B. Normand, *Electrochem. Commun.*, 26 (2013) 10.
48. E.M. Martini and I.L. Muller, *Corros. Sci.*, 42 (2000) 443.
49. D. Yavas, P. Mishra, A. Alshehri, P. Shrotriya, K.R. Hebert and A.F. Bastawros, *Electrochem. Commun.*, 88 (2018) 88.
50. M. Kermani and A. Morshed, *Corrosion*, 59 (2003) 659.
51. B. Linter and G. Burstein, *Corros. Sci.*, 41 (1999) 117.
52. M. Keddad, O.R. Mattos and H. Takenouti, *J. Electrochem. Soc.*, 128 (1981) 257.
53. M. Keddad, O.R. Mattos and H. Takenouti, *J. Electrochem. Soc.*, 128 (1981) 266.

© 2019 The Authors. Published by ESG (www.electrochemsci.org). This article is an open access article distributed under the terms and conditions of the Creative Commons Attribution license (<http://creativecommons.org/licenses/by/4.0/>).